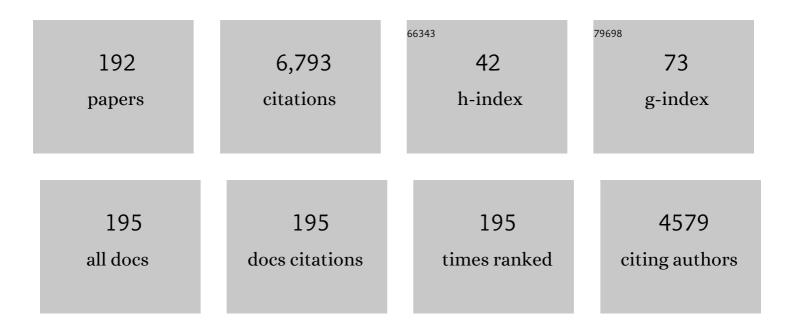
T James Marrow

List of Publications by Year in descending order

Source: https://exaly.com/author-pdf/536419/publications.pdf Version: 2024-02-01



T IMES MADDOW

#	Article	IF	CITATIONS
1	In Situ Mechanical Loading and Neutron Bragg-edge Imaging, Applied to Polygranular Graphite On IMAT@ISIS. Experimental Mechanics, 2022, 62, 59-73.	2.0	0
2	High temperature spherical nano-indentation of graphite crystals. Carbon, 2022, 191, 236-242.	10.3	14
3	Crack field analysis by optical DIC of short cracks in Zircaloy-4. Procedia Structural Integrity, 2022, 39, 663-670.	0.8	4
4	Combined evaluation of Young modulus and fracture toughness in small specimens of fine grained nuclear graphite using 3D image analysis. Journal of Nuclear Materials, 2022, 563, 153642.	2.7	10
5	Crack propagation in fine grained graphites under mode I and mixed-mode loading, as observed in situ by microtomography. Carbon, 2022, 193, 356-367.	10.3	8
6	Achieving Ultrahighâ€Rate Planar and Dendriteâ€Free Zinc Electroplating for Aqueous Zinc Battery Anodes. Advanced Materials, 2022, 34, e2202552.	21.0	88
7	Effect of irradiation swelling on the mechanical properties of unidirectional SiC/SiC composites: A numerical investigation at microstructural level. Journal of Nuclear Materials, 2022, 569, 153918.	2.7	7
8	Imaging Sodium Dendrite Growth in Allâ€5olidâ€5tate Sodium Batteries Using ²³ Na <i>T</i> ₂ â€Weighted Magnetic Resonance Imaging. Angewandte Chemie - International Edition, 2021, 60, 2110-2115.	13.8	21
9	Effects of polymer infiltration processing (PIP) temperature on the mechanical and thermal properties of Nextel 312 fibre SiCO ceramic matrix composites. Composites Part A: Applied Science and Manufacturing, 2021, 140, 106197.	7.6	6
10	Imaging Sodium Dendrite Growth in Allâ€Solidâ€State Sodium Batteries Using 23 Na T 2 â€Weighted Magnetic Resonance Imaging. Angewandte Chemie, 2021, 133, 2138-2143.	2.0	2
11	A Robust Finite Element-based Filter for Digital Image and Volume Correlation Displacement Data. Experimental Mechanics, 2021, 61, 901.	2.0	5
12	Comparison of ultrafine-grain isotropic graphite prepared from microcrystalline graphite and pitch coke. Fuel, 2021, 290, 120055.	6.4	14
13	Visualizing plating-induced cracking in lithium-anode solid-electrolyte cells. Nature Materials, 2021, 20, 1121-1129.	27.5	221
14	Temperature Dependence of Lithium Anode Voiding in Argyrodite Solid-State Batteries. ACS Applied Materials & Interfaces, 2021, 13, 22708-22716.	8.0	38
15	In situ X-ray tomography characterisation of 3D deformation of C/C-SiC composites loaded under tension. Composites Part A: Applied Science and Manufacturing, 2021, 145, 106390.	7.6	22
16	The infiltration behavior and chemical compatibility of molten lead-bismuth eutectic in nuclear graphite at elevated temperature. Journal of Nuclear Materials, 2021, 550, 152921.	2.7	0
17	Measurements by x-ray diffraction of the temperature dependence of lattice parameter and crystallite size for isostatically-pressed graphite. Carbon Trends, 2021, 4, 100071.	3.0	18
18	In situ observation of the deformation and fracture of an alumina-alumina ceramic-matrix composite at elevated temperature using x-ray computed tomography. Journal of the European Ceramic Society, 2021, 41, 4217-4230.	5.7	20

#	Article	IF	CITATIONS
19	J-integral analysis of the elastic strain fields of ferrite deformation twins using electron backscatter diffraction. Acta Materialia, 2021, 218, 117203.	7.9	12
20	In situ investigation of failure in 3D braided SiCf/SiC composites under flexural loading. Composite Structures, 2021, 270, 114067.	5.8	19
21	Ex-situ micro X-ray computed tomography tests and image-based simulation of UHPFRC beams under bending. Cement and Concrete Composites, 2021, 123, 104216.	10.7	13
22	A new method for predicting susceptibility of austenitic stainless steels to intergranular stress corrosion cracking. Materials and Design, 2020, 187, 108368.	7.0	20
23	Sodium/Na β″ Alumina Interface: Effect of Pressure on Voids. ACS Applied Materials & Interfaces, 2020, 12, 678-685.	8.0	86
24	Characterisation of slip and twin activity using digital image correlation and crystal plasticity finite element simulation: Application to orthorhombic l±-uranium. Journal of the Mechanics and Physics of Solids, 2020, 135, 103800.	4.8	20
25	A method for fracture toughness measurement in trabecular bone using computed tomography, image correlation and finite element methods. Journal of the Mechanical Behavior of Biomedical Materials, 2020, 109, 103838.	3.1	13
26	In situ measurement of elastic and total strains during ambient and high temperature deformation of a polygranular graphite. Carbon, 2020, 163, 308-323.	10.3	15
27	A 3D fullâ€field study of cracks in a nuclear graphite under mode I and mode II cyclic dwell loading conditions. Fatigue and Fracture of Engineering Materials and Structures, 2020, 43, 1646-1657.	3.4	4
28	3D finite element modeling of water diffusion behavior of jute/PLA composite based on X-ray computed tomography. Composites Science and Technology, 2020, 199, 108313.	7.8	17
29	Measuring the brittle-to-ductile transition temperature of tungsten–tantalum alloy using chevron-notched micro-cantilevers. Scripta Materialia, 2020, 180, 77-82.	5.2	15
30	Analysis of Interfacial Effects in All-Solid-State Batteries with Thiophosphate Solid Electrolytes. ACS Applied Materials & Interfaces, 2020, 12, 9277-9291.	8.0	73
31	Procedure for accurate calculation of the <i>J</i> â€integral from digital volume correlation displacement data. Strain, 2020, 56, e12337.	2.4	7
32	J-integral analysis: An EDXD and DIC comparative study for a fatigue crack. International Journal of Fatigue, 2020, 134, 105474.	5.7	17
33	Unifying the effects of in and out-of-plane constraint on the fracture of ductile materials. Journal of the Mechanics and Physics of Solids, 2020, 141, 103956.	4.8	21
34	Fatigue crack closure: A myth or a misconception?. Fatigue and Fracture of Engineering Materials and Structures, 2019, 42, 2747-2763.	3.4	29
35	Critical stripping current leads to dendrite formation on plating in lithium anode solid electrolyte cells. Nature Materials, 2019, 18, 1105-1111.	27.5	592
36	Validating 3D two-parameter fracture mechanics models for structural integrity assessments. Theoretical and Applied Fracture Mechanics, 2019, 103, 102281.	4.7	3

#	Article	IF	CITATIONS
37	Evaluation of Fracture Toughness Measurements Using Chevron-Notched Silicon and Tungsten Microcantilevers. Jom, 2019, 71, 3378-3389.	1.9	13
38	Microstructure Characterization by X-Ray Computed Tomography of C/C-SiC Ceramic Composites Fabricated with Different Carbon Fiber Architectures. Applied Composite Materials, 2019, 26, 1247-1260.	2.5	14
39	Application of neutron imaging to detect and quantify fatigue cracking. International Journal of Mechanical Sciences, 2019, 159, 182-194.	6.7	19
40	Structure and flexural properties of 3D needled carbon fiber reinforced carbon and silicon carbide (C/C-SiC) composites fabricated by gaseous and liquid silicon infiltration. Ceramics International, 2019, 45, 17978-17986.	4.8	22
41	Computed tomography porosity and spherical indentation for determining cortical bone millimetre-scale mechanical properties. Scientific Reports, 2019, 9, 7416.	3.3	22
42	Damage development during flexural loading of a 5-directional braided C/C-SiC composite, characterized by X-ray tomography and digital volume correlation. Ceramics International, 2019, 45, 5601-5612.	4.8	24
43	Hygrothermal aging and structural damage of a jute/poly (lactic acid) (PLA) composite observed by X-ray tomography. Composites Science and Technology, 2019, 173, 15-23.	7.8	48
44	In situ observation of compression damage in a 3D needled-punched carbon fiber-silicon carbide ceramic matrix composite. Composite Structures, 2019, 210, 189-201.	5.8	36
45	Mesoscopic structure features in synthetic graphite. Materials and Design, 2018, 142, 268-278.	7.0	37
46	Lattice strain and texture development in coarse-grained uranium – a neutron diffraction study. Journal of Physics: Conference Series, 2018, 1106, 012012.	0.4	5
47	Validating 3D two-parameter fracture mechanics for structural integrity assessments. Procedia Structural Integrity, 2018, 13, 965-970.	0.8	2
48	Data related to the mesoscopic structure of iso-graphite for nuclear applications. Data in Brief, 2018, 19, 651-659.	1.0	4
49	In situ mapping of normal strains in the field of a growing fatigue crack in a steel weld using digital image correlation and energy dispersive synchrotron X-ray diffraction. International Journal of Fatigue, 2018, 115, 11-19.	5.7	6
50	In situ Observation of Compression Damage in a Three-Dimensional Braided Carbon Fiber Reinforced Carbon and Silicon Carbide (C/C-SiC) Ceramic Composite. Microscopy and Microanalysis, 2018, 24, 227-237.	0.4	12
51	J-Integral Calculation by Finite Element Processing of Measured Full-Field Surface Displacements. Experimental Mechanics, 2017, 57, 997-1009.	2.0	47
52	An autonomous surface discontinuity detection and quantification method by digital image correlation and phase congruency. Optics and Lasers in Engineering, 2017, 96, 94-106.	3.8	49
53	A multi-scale three-dimensional Cellular Automata fracture model of radiolytically oxidised nuclear graphite. Carbon, 2017, 121, 574-590.	10.3	12
54	Synchrotron X-ray characterization of crack strain fields in polygranular graphite. Carbon, 2017, 124, 357-371.	10.3	45

#	Article	IF	CITATIONS
55	Observation of crack growth in a polycrystalline ferroelectric by synchrotron X-ray diffraction. Scripta Materialia, 2017, 140, 23-26.	5.2	5
56	3D Cellular Automata fracture model for porous graphite microstructures. Nuclear Engineering and Design, 2017, 323, 202-208.	1.7	7
57	Threeâ€dimensional measurement and cohesive element modelling of deformation and damage in a 2.5â€dimensional woven ceramic matrix composite. Fatigue and Fracture of Engineering Materials and Structures, 2017, 40, 683-695.	3.4	9
58	In-situ X-ray computed tomography characterisation of 3D fracture evolution and image-based numerical homogenisation of concrete. Cement and Concrete Composites, 2017, 75, 74-83.	10.7	161
59	Effect of surface machining on intergranular stress corrosion cracking (IGSCC) in sensitised type 304 austenitic stainless steel. Corrosion Engineering Science and Technology, 2016, 51, 383-391.	1.4	15
60	Quantifying yield behaviour in metals by X-ray nanotomography. Scientific Reports, 2016, 6, 34346.	3.3	15
61	Porosity characterization of fiber-reinforced ceramic matrix composite using synchrotron X-ray computed tomography. Journal of Instrumentation, 2016, 11, C03052-C03052.	1.2	16
62	Obtaining the J-integral by diffraction-based crack-field strain mapping. Procedia Structural Integrity, 2016, 2, 2519-2526.	0.8	12
63	Multifractal-based assessment of Gilsocarbon graphite microstructures. Carbon, 2016, 109, 711-718.	10.3	14
64	In situ observation of mechanical damage within a SiC-SiC ceramic matrix composite. Journal of Nuclear Materials, 2016, 481, 13-23.	2.7	67
65	Multi-scale damage modelling in a ceramic matrix composite using a finite-element microstructure meshfree methodology. Philosophical Transactions Series A, Mathematical, Physical, and Engineering Sciences, 2016, 374, 20150276.	3.4	14
66	Multi-scale modelling of nuclear graphite tensile strength using the site-bond lattice model. Carbon, 2016, 100, 273-282.	10.3	12
67	Time-resolved synchrotron tomographic quantification of deformation during indentation of an equiaxed semi-solid granular alloy. Acta Materialia, 2016, 105, 338-346.	7.9	40
68	Three-dimensional displacement mapping of diffused Pt thermal barrier coatings via synchrotron X-ray computed tomography and digital volume correlation. Scripta Materialia, 2016, 115, 100-103.	5.2	13
69	Observation and simulation of indentation damage in a SiC–SiCfibre ceramic matrix composite. Finite Elements in Analysis and Design, 2016, 110, 11-19.	3.2	23
70	In situ measurement of the strains within a mechanically loaded polygranular graphite. Carbon, 2016, 96, 285-302.	10.3	51
71	Plasma-sprayed thermal barrier coatings: numerical study on damage localization and evolution. Frattura Ed Integrita Strutturale, 2016, 10, 322-329.	0.9	0
72	FEMME: A multi-scale Finite Element Microstructure MEshfree fracture model for quasi-brittle materials with complex microstructures. Engineering Fracture Mechanics, 2015, 147, 355-372.	4.3	18

#	Article	IF	CITATIONS
73	Synchrotron X-ray Tomographic Quantification of Deformation Induced Strain Localisation in Semi-solid Al- 15wt.%Cu. IOP Conference Series: Materials Science and Engineering, 2015, 84, 012079.	0.6	4
74	Time-resolved synchrotron tomographic quantification of deformation-induced flow in a semi-solid equiaxed dendritic Al–Cu alloy. Scripta Materialia, 2015, 103, 69-72.	5.2	23
75	Multi-scale modeling of damage development in a thermal barrier coating. Surface and Coatings Technology, 2015, 276, 399-407.	4.8	26
76	Method for the explicit insertion of microstructure in Cellular Automata Finite Element (CAFE) models based on an irregular tetrahedral Finite Element mesh: Application in a multi-scale Finite Element Microstructure MEshfree framework (FEMME). Finite Elements in Analysis and Design, 2015, 105, 56-62.	3.2	13
77	Influence of milling on the development of stress corrosion cracks in austenitic stainless steel. Journal of Materials Processing Technology, 2015, 218, 32-37.	6.3	57
78	Yield behavior beneath hardness indentations in ductile metals, measured by three-dimensional computed X-ray tomography and digital volume correlation. Acta Materialia, 2015, 82, 468-482.	7.9	67
79	Advanced 2D and 3D Digital Image Correlation of the Full-Field Displacements of Cracks and Defects. , 2015, , 56-69.		3
80	RICH TOMOGRAPHY TECHNIQUES FOR THE ANALYSIS OF MICROSTRUCTURE AND DEFORMATION. International Journal of Computational Methods, 2014, 11, 1343006.	1.3	10
81	FAFNIR: Strategy and risk reduction in accelerator driven neutron sources for fusion materials irradiation data. Fusion Engineering and Design, 2014, 89, 2108-2113.	1.9	11
82	Reducing risk and accelerating delivery of a neutron source for fusion materials research. Fusion Engineering and Design, 2014, 89, 273-279.	1.9	5
83	Grain boundary structure and intergranular stress corrosion crack initiation in high temperature water of a thermally sensitised austenitic stainless steel, observed in situ. Corrosion Science, 2014, 85, 428-435.	6.6	80
84	3D Cellular Automata Finite Element Method with Explicit Microstructure: Modeling Quasi-brittle Fracture using Meshfree Damage Propagation. , 2014, 3, 1143-1148.		12
85	3D Studies of Damage by Combined X-ray Tomography and Digital Volume Correlation. , 2014, 3, 1554-1559.		17
86	In situ synchrotron tomographic quantification of granular and intragranular deformation during semi-solid compression of an equiaxed dendritic Al–Cu alloy. Acta Materialia, 2014, 76, 371-380.	7.9	84
87	A quantitative three-dimensional in situ study of a short fatigue crack in a magnesium alloy. International Journal of Fatigue, 2014, 66, 183-193.	5.7	34
88	In situ quantitative three-dimensional characterisation of sub-indentation cracking in polycrystalline alumina. Journal of the European Ceramic Society, 2014, 34, 3127-3132.	5.7	30
89	Flexural strength and defect behaviour of polygranular graphite under different states of stress. Carbon, 2013, 59, 325-336.	10.3	43
90	Three-dimensional observation and image-based modelling of thermal strains in polycrystalline alumina. Acta Materialia, 2013, 61, 7521-7533.	7.9	18

#	Article	IF	CITATIONS
91	Annealing of ion irradiation damage in nuclear graphite. Journal of Nuclear Materials, 2013, 434, 334-346.	2.7	25
92	Three-dimensional crack observation, quantification and simulation in a quasi-brittle material. Acta Materialia, 2013, 61, 6276-6289.	7.9	62
93	Application of accelerator based neutron sources in fusion materials research. , 2013, , .		4
94	In situ observation of short fatigue crack propagation in oxygenated water at elevated temperature and pressure. Corrosion Science, 2013, 68, 34-43.	6.6	29
95	Observation and quantification of three-dimensional crack propagation in poly-granular graphite. Engineering Fracture Mechanics, 2013, 110, 410-420.	4.3	64
96	Effects of orientation, stress and exposure time on short intergranular stress corrosion crack behaviour in sensitised type 304 austenitic stainless steel. Fatigue and Fracture of Engineering Materials and Structures, 2012, 35, 359-373.	3.4	18
97	Intergranular crack nuclei in polycrystalline alumina. Engineering Fracture Mechanics, 2012, 95, 29-36.	4.3	8
98	Fracture behaviour of an anisotropic polygranular graphite (PGA). Materials Science & Engineering A: Structural Materials: Properties, Microstructure and Processing, 2012, 558, 265-277.	5.6	26
99	Detection and characterisation of intergranular stressâ€corrosion cracking on austenitic stainless steel. Materials and Corrosion - Werkstoffe Und Korrosion, 2012, 63, 664-673.	1.5	9
100	Application of an independent parallel reactions model on the annealing kinetics of BEPO irradiated graphite. Journal of Nuclear Materials, 2012, 427, 95-109.	2.7	5
101	Quantitative <i>in situ</i> study of short crack propagation in polygranular graphite by digital image correlation. Fatigue and Fracture of Engineering Materials and Structures, 2012, 35, 695-707.	3.4	39
102	An approach to calculate the <i>J</i> â€integral by digital image correlation displacement field measurement. Fatigue and Fracture of Engineering Materials and Structures, 2012, 35, 971-984.	3.4	159
103	A new approach for DL-EPR testing of thermo-mechanically processed austenitic stainless steel. Corrosion Science, 2011, 53, 4213-4222.	6.6	33
104	Diffraction contrast tomography for the study of polycrystalline stainless steel microstructures and stress corrosion cracking. Revue De Metallurgie, 2011, 108, 47-50.	0.3	2
105	A method for the 3-D quantification of bridging ligaments during crack propagation. Scripta Materialia, 2011, 65, 131-134.	5.2	15
106	In situ observation of crack nuclei in poly-granular graphite under ring-on-ring equi-biaxial and flexural loading. Engineering Fracture Mechanics, 2011, 78, 1756-1770.	4.3	32
107	Three-dimensional in situ observations of short fatigue crack growth in magnesium. Acta Materialia, 2011, 59, 6761-6771.	7.9	114
108	3-D growth of a short fatigue crack within a polycrystalline microstructure studied using combined diffraction and phase-contrast X-ray tomography. Acta Materialia, 2011, 59, 590-601.	7.9	166

#	Article	IF	CITATIONS
109	An Evaluation of the Double Torsion Technique. Experimental Mechanics, 2011, 51, 1511-1526.	2.0	20
110	Damage, crack growth and fracture characteristics of nuclear grade graphite using the Double Torsion technique. Journal of Nuclear Materials, 2011, 414, 32-43.	2.7	63
111	Preliminary Evaluation of Digital Image Correlation for In-situ Observation of Low Temperature Atmospheric-Induced Chloride Stress Corrosion Cracking in Austenitic Stainless Steels. ECS Transactions, 2010, 25, 119-132.	0.5	27
112	Characterization of polycrystalline materials using synchrotron X-ray imaging and diffraction techniques. Jom, 2010, 62, 22-28.	1.9	42
113	Nanotomography for understanding materials degradation. Scripta Materialia, 2010, 63, 835-838.	5.2	45
114	Non-destructive analysis of micro texture and grain boundary character from X-ray diffraction contrast tomography. Nuclear Instruments & Methods in Physics Research B, 2010, 268, 291-296.	1.4	25
115	Towards Understanding the Development of Grain Boundary Clusters in Austenitic Stainless Steel. Materials Science Forum, 2010, 638-642, 3206-3211.	0.3	2
116	Mechanical Properties and Fracture of Materials. , 2010, , 77-88.		1
117	Fracture behaviour of radiolytically oxidised reactor core graphites: A view. Materials Science and Technology, 2010, 26, 899-907.	1.6	44
118	Characterisation of grain boundary cluster compactness in austenitic stainless steel. Materials Science and Technology, 2010, 26, 670-675.	1.6	13
119	Correlations of electrochemical noise, acoustic emission and complementary monitoring techniques during intergranular stress-corrosion cracking of austenitic stainless steel. Corrosion Science, 2010, 52, 2015-2025.	6.6	114
120	3D inspection of fabrication and degradation processes from X-ray (micro) tomography images using a hole closing algorithm. , 2010, , .		1
121	Fiveâ€parameter grain boundary analysis of a grain boundary–engineered austenitic stainless steel. Journal of Microscopy, 2009, 233, 417-422.	1.8	18
122	<i>In situ</i> observation of intergranular crack nucleation in a grain boundary controlled austenitic stainless steel. Journal of Microscopy, 2009, 233, 423-431.	1.8	52
123	New opportunities for 3D materials science of polycrystalline materials at the micrometre lengthscale by combined use of X-ray diffraction and X-ray imaging. Materials Science & Engineering A: Structural Materials: Properties, Microstructure and Processing, 2009, 524, 69-76.	5.6	164
124	Three-dimensional grain mapping by x-ray diffraction contrast tomography and the use of Friedel pairs in diffraction data analysis. Review of Scientific Instruments, 2009, 80, 033905.	1.3	223
125	Towards Modelling Intergranular Stress-Corrosion Cracks Using Experimentally Obtained Grain Topologies. , 2009, , .		3
126	Microstructural characterisation of nuclear grade graphite. Journal of Nuclear Materials, 2008, 381, 152-157.	2.7	43

#	Article	IF	CITATIONS
127	Surface grain boundary engineering of shot-peened type 304 stainless steel. Journal of Materials Science, 2008, 43, 1270-1277.	3.7	19
128	X-ray diffraction contrast tomography: a novel technique for three-dimensional grain mapping of polycrystals. II. The combined case. Journal of Applied Crystallography, 2008, 41, 310-318.	4.5	159
129	Preparation of fatigue specimens with controlled surface characteristics. Journal of Materials Processing Technology, 2008, 203, 396-403.	6.3	13
130	Analysis of crack propagation in nuclear graphite using three-point bending of sandwiched specimens. Journal of Nuclear Materials, 2008, 372, 141-151.	2.7	38
131	Microstructural modelling of nuclear graphite using multi-phase models. Journal of Nuclear Materials, 2008, 380, 46-58.	2.7	27
132	Microcracks in nuclear graphite and highly oriented pyrolytic graphite (HOPG). Journal of Nuclear Materials, 2008, 381, 199-203.	2.7	83
133	Microstructural scale strain localisation in nuclear graphite. Journal of Nuclear Materials, 2008, 381, 171-176.	2.7	7
134	Failure analysis of the effects of porosity in thermally oxidised nuclear graphite using finite element modelling. Journal of Nuclear Materials, 2008, 381, 1-8.	2.7	26
135	Application of an independent parallel reactions model on the annealing kinetics to irradiated graphite waste. Journal of Nuclear Materials, 2008, 381, 83-91.	2.7	7
136	Characterization of heterogeneity and nonlinearity in material properties of nuclear graphite using an inverse method. Journal of Nuclear Materials, 2008, 381, 158-164.	2.7	5
137	The microstructure of nuclear graphite binders. Carbon, 2008, 46, 62-71.	10.3	83
138	Three-dimensional characterization and thermal property modelling of thermally oxidized nuclear graphite. Acta Materialia, 2008, 56, 4242-4254.	7.9	24
139	Observation of microstructure deformation and damage in nuclear graphite. Engineering Fracture Mechanics, 2008, 75, 3633-3645.	4.3	46
140	Modelling the effects of surface finish on fatigue limit in austenitic stainless steels. Fatigue and Fracture of Engineering Materials and Structures, 2008, 31, 581-598.	3.4	15
141	The influence of lowâ€strain thermoâ€mechanical processing on grain boundary network characteristics in type 304 austenitic stainless steel. Journal of Microscopy, 2008, 230, 435-444.	1.8	32
142	Effect of thermomechanical process history on grain boundary control in an austenitic stainless steel. Scripta Materialia, 2008, 59, 554-557.	5.2	31
143	Mesoscale Mechanical Model for Intergranular Stress Corrosion Cracking and Implications for Microstructure Engineering. Journal of Pressure Vessel Technology, Transactions of the ASME, 2008, 130, .	0.6	6
144	Observations of Intergranular Stress Corrosion Cracking in a Grain-Mapped Polycrystal. Science, 2008, 321, 382-385.	12.6	406

#	Article	IF	CITATIONS
145	Nanostructures of carbon in nuclear graphite. Journal of Physics: Conference Series, 2008, 126, 012056.	0.4	2
146	In-Situ Observations of Intergranular Stress Corrosion Cracking. , 2008, , .		6
147	Grain boundary engineering for crack bridging. , 2008, , 69-79.		6
148	High-resolution, in-situ, tomographic observations of stress corrosion cracking. , 2008, , 439-447.		10
149	In-Situ Observation of Crack Nucleation in Nuclear Graphite by Digital Image Correlation. , 2008, , .		5
150	Rates of intergranular environment assisted cracking in three-dimensional model microstructures. Theoretical and Applied Fracture Mechanics, 2007, 48, 187-202.	4.7	25
151	X-ray tomography observation of crack propagation in nuclear graphite. Materials Science and Technology, 2006, 22, 1045-1051.	1.6	54
152	A three-dimensional computational model for intergranular cracking. Computational Materials Science, 2006, 38, 442-453.	3.0	44
153	Measurement of crack bridging stresses in environment-assisted cracking of duplex stainless by synchrotron diffraction. Fatigue and Fracture of Engineering Materials and Structures, 2006, 29, 464-471.	3.4	10
154	A two-dimensional mesoscale model for intergranular stress corrosion crack propagationâ~†. Acta Materialia, 2006, 54, 3493-3501.	7.9	35
155	Numerical modelling of the effects of porosity changes on the mechanical properties of nuclear graphite. Journal of Nuclear Materials, 2006, 352, 1-5.	2.7	51
156	Three dimensional observations and modelling of intergranular stress corrosion cracking in austenitic stainless steel. Journal of Nuclear Materials, 2006, 352, 62-74.	2.7	108
157	In situ analysis of cracks in structural materials using synchrotron X-ray tomography and diffraction. Nuclear Instruments & Methods in Physics Research B, 2006, 246, 217-225.	1.4	52
158	Mapping the evolution of density in 3D of thermally oxidised graphite for nuclear applications. Scripta Materialia, 2006, 54, 829-834.	5.2	21
159	Meso-Scale Mechanical Model for Intergranular Stress Corrosion Cracking and Implications for Microstructure Engineering. , 2006, , 591.		0
160	Characterization of Material Properties Using an Inverse Method. Applied Mechanics and Materials, 2006, 5-6, 107-114.	0.2	5
161	X-ray microtomography studies of localised corrosion and transitions to stress corrosion cracking. Materials Science and Technology, 2006, 22, 1076-1085.	1.6	81
162	X-ray microtomographic observation of intergranular stress corrosion cracking in sensitised austenitic stainless steel. Materials Science and Technology, 2006, 22, 1068-1075.	1.6	91

#	Article	IF	CITATIONS
163	Environment-Assisted Cracking of High-Strength Magnesium Alloys WE43-T6. , 2006, , 893-894.		0
164	Effects of Surface Finish on the Fatigue Limit in Austenitic Stainless Steels (Modelling and) Tj ETQq0 0 0 rgBT /Ov	erlock 10	Tf ₀ 50 702 To
165	The effect of thermal oxidation on polycrystalline graphite studied by X-ray tomography. Carbon, 2005, 43, 765-774.	10.3	51
166	Controlled Initiation of Short Fatigue Cracks in 316L Steel. , 2005, , .		0
167	High resolution X-ray tomography of short fatigue crack nucleation in austempered ductile cast iron. International Journal of Fatigue, 2004, 26, 717-725.	5.7	91
168	Environment-assisted cracking of cast WE43-T6 magnesium. Materials Science & Engineering A: Structural Materials: Properties, Microstructure and Processing, 2004, 387-389, 419-423.	5.6	28
169	Fatigue crack nuclei in austempered ductile cast iron. Fatigue and Fracture of Engineering Materials and Structures, 2002, 25, 635-648.	3.4	17
170	Short fatigue cracks in austempered ductile cast iron (ADI). Fatigue and Fracture of Engineering Materials and Structures, 2000, 23, 425-434.	3.4	26
171	The Internet Microscope Materials Research Society Symposia Proceedings, 2000, 632, 1.	0.1	0
172	Application of electron backscattered diffraction to cleavage fracture in duplex stainless steel. Scripta Materialia, 1999, 40, 1395-1400.	5.2	14
173	THE BRITTLE FRACTURE OF 475°C EMBRITTLED CAST DUPLEX STAINLESS STEEL. Fatigue and Fracture of Engineering Materials and Structures, 1997, 20, 565-571.	3.4	4
174	THE CRACK INITIATION TOUGHNESS FOR BRITTLE FRACTURE OF SUPER DUPLEX STAINLESS STEEL. Fatigue and Fracture of Engineering Materials and Structures, 1997, 20, 1005-1014.	3.4	6
175	Hydrogen-assisted stable crack growth in iron-3 wt% silicon steel. Acta Materialia, 1996, 44, 3125-3140.	7.9	34
176	THE FRACTURE MECHANISM IN 475°C EMBRITTLED FERRITIC STAINLESS STEELS. Fatigue and Fracture of Engineering Materials and Structures, 1996, 19, 919-933.	3.4	14
177	THE FRACTURE MECHANISM OF 475°C EMBRITTLEMENT IN A DUPLEX STAINLESS STEEL. Fatigue and Fracture of Engineering Materials and Structures, 1996, 19, 935-947.	3.4	11
178	Fatigue crack propagation mechanisms in a thermally aged duplex stainless steel. Materials Science & Engineering A: Structural Materials: Properties, Microstructure and Processing, 1994, 183, 91-101.	5.6	19
179	Toughening mechanisms in the high temperature fracture of high purity alumina. Materials Science & Engineering A: Structural Materials: Properties, Microstructure and Processing, 1994, 176, 455-460.	5.6	0

180The brittle/ductile transition in cubic stabilised zirconia. Journal of the European Ceramic Society,
1994, 14, 447-453.5.716

#	Article	IF	CITATIONS
181	In-situ scanning acoustic microscopy of crack bridging in alumina. Journal of the European Ceramic Society, 1994, 14, 111-116.	5.7	9
182	MICROSTRUCTURAL AND ENVIRONMENTAL EFFECTS ON FATIGUE CRACK PROPAGATION IN DUPLEX STAINLESS STEELS. Fatigue and Fracture of Engineering Materials and Structures, 1994, 17, 761-771.	3.4	28
183	Scanning Acoustic Microscopy Observations of High-Temperature Crack-Bridging Mechanisms in Alumina. Journal of the American Ceramic Society, 1993, 76, 2915-2918.	3.8	8
184	Temperature effects on the mechanism of time independent hydrogen assisted fatigue crack propagation in steels. Acta Metallurgica Et Materialia, 1992, 40, 2059-2068.	1.8	31
185	Effect of mean stress on hydrogen assisted fatique crack propagation in duplex stainless steel. Acta Metallurgica Et Materialia, 1991, 39, 1367-1376.	1.8	29
186	Grain Tracking at the High Energy Materials Science Beamline of the Petra III Synchrotron Radiation Source. Materials Science Forum, 0, 652, 70-73.	0.3	2
187	<i>In-Situ</i> Observation and Modelling of Intergranular Cracking in Polycrystalline Alumina. Key Engineering Materials, 0, 465, 560-563.	0.4	1
188	Influence of Twins on Short Fatigue Cracks in Type 316L Stainless Steel. Key Engineering Materials, 0, 465, 507-510.	0.4	6
189	Fracture Characterisation of Reactor Core Graphite under Biaxial Loading. Key Engineering Materials, 0, 577-578, 485-488.	0.4	0
190	3D Studies of Indentation by Combined X-Ray Tomography and Digital Volume Correlation. Key Engineering Materials, 0, 592-593, 14-21.	0.4	77
191	Studying SiC/SiC Composites by X-Ray Tomography. Key Engineering Materials, 0, 602-603, 416-421.	0.4	5
192	Effect of Strain Path and Annealing on Development of Resistance to Intergranular Degradation in Austenitic Stainless Steels. Ceramic Transactions, 0, , 323-334.	0.1	2